Few-Body Syst. manuscript No.
(will be inserted by the editor)

Universal prohibited zones in the coordinate space of few-body systems

C. G. Bao*

Received: date / Accepted: date

Abstract In some special zones of the high-dimensional coordinate space of few-body systems with identical particles, the operation of an element (or a product of elements) of the symmetry groups of the Hamiltonian on a quantum state might be equivalent to the operation of another element. Making use of the matrix representations of the groups, the equivalence leads to a set of homogeneous linear equations imposing on the wave functions. When the matrix of these equations is non-degenerate, the wave functions will appear as nodal surfaces in these zones. In this case, these zones are prohibited. In this paper, tightly bound 4-boson systems with three types of interaction have been studied analytically and numerically. The existence of the universal prohibited zones has been revealed, and their decisive effect on the structures of the eigenstates is demonstrated.

PACS 03.65.-w · 03.65.Ge · 02.20.-a · 21.45.-v · 36.40.Mr

1 Introduction

Since various systems may be governed by the same fundamental law, universality exists in nature. The early indications of universality in quantum mechanic three-body systems was discovered before 1970.[1,2,3] The first strong evidence was given by Efimov in 1970 on three weakly bound identical bosons.[4,5] He found that, when the scattering length is sufficiently long, a sequence of loosely bound states, the "Efimov states", will appear. The properties of these states are governed by a universal law, not depend on the dynamic details of the 3-boson systems. In this paper, another kind of universality that exists in tightly bound quantum mechanic few-body systems is revealed and confirmed numerically.

The Hamiltonian of identical particles is invariant under the operations of a set of symmetry groups G_α, G_β, $\cdots$ (including the permutation group).[6,7,8,9] Consequently, the eigenstates $\{\Psi_i(X)\}$ are classified according to the representations of these

* Email: stsbcg@mail.sysu.edu.cn

State Key Laboratory of Optoelectronic Materials and Technologies, School of Physics and Engineering, Sun Yat-Sen University, Guangzhou, 510275, P.R. China

groups, where X denotes a set of coordinates and i is a serial number. Let g_α be an element of G_α, g_β be that of G_β, and Ξ denotes a special zone in the high-dimensional coordinate space. When $X \in \Xi$, the effects of g_α and g_β might be equivalent so that $g_\alpha \Psi_i(X) = g_\beta \Psi_i(X)$. For an example, when Ξ is the zone of the squares (SQ), g_α is a rotation about the normal of the SQ by $2\pi/4$, and g_β is a cyclic permutation of particles, then g_α and g_β are equivalent in Ξ. Making use of the representations of groups, the equivalence leads to a set of homogeneous linear equations

$$\sum_{i'} [D^{\alpha}_{i'i}(g_\alpha) - D^{\beta}_{i'i}(g_\beta)] \Psi_{i'}(X) = 0, \quad (X \in \Xi), \tag{1}$$

where $D^{\alpha}_{i'i}(g_\alpha)$ are the matrix elements of the representation. When the matrix of this set of equations is non-degenerate, the set $\Psi_{i'}(X)$ must be zero in Ξ. In this case, Ξ becomes a prohibited zone (PZ) and the wave function appears as an inherent nodal surface (INS).[10] Eq. (1) demonstrates that, for each pair of equivalent operations, a constraint will be imposed on the eigenstates. Since the matrixes of representations are absolutely irrelevant to dynamics, the constraint is universal disregarding the kind of systems (nuclear, atomic, or molecular) and the details of dynamic parameters. It implies that the states of different systems but belonging to the same set of representations will have exactly the same PZ, and their wave functions will have exactly the same INS. On the other hand, some zones are important to binding (say, for 4-body systems, the zones of equilateral tetrahedron (ET) and SQ). Whether these zones are prohibited is crucial to the binding energy and the geometric character of a state. Furthermore, the number and the locations of the nodal surfaces in a wave function in general determine the strength and mode of oscillation. In particular, the existence of the INS implies an inherent mode. Thus, the eigenstates would be seriously affected by the universal symmetry constraint.

The decisive effect of the symmetry constraint on the triply and quadruple excited intrashell states of atoms has been revealed previously.[11,12,13,14,15] Accordingly, these states can be naturally classified according to their inherent nodal structures.[16, 17] For 4-boson systems, a number of predictions on the structures and internal modes of oscillation have been made previously.[18,19] However, these predictions have not yet been confirmed numerically. The present paper generalizes the work of [18,19] in the following aspects: (i) Instead of free 4-boson systems, trapped 4-boson systems are considered. Thereby a number of tightly bound states can be obtained which are necessary for a systematic analysis. (ii) In addition to theoretical analysis, numerical calculations have been performed so that the effect of symmetry constraint can be appraised quantitatively. (iii) Three types of interactions have been adopted. The aim is to demonstrate the similarity among different kinds of systems.

In the next section, the symmetry constraints imposing on 4-boson systems are studied theoretically. We have chosen appropriate sets of coordinates so that Eq. (1) appears in very simple forms and the analysis becomes transparent. Then, an isotropic trap together with three types of interaction are introduced, and numerical calculations are performed to diagonalize the Hamiltonian. Under the trap the total orbital angular momentum L, its Z-component M, and the parity Π are good quantum numbers. Accordingly, an eigenstate with the c.m. motion removed can be denoted as $\Psi^{\Pi}_{LM,i}$, where i denotes the i-th state of a L^{Π}-series. Mostly the $i = 1$ states (the lowest one) are concerned. Therefore, the label i is dropped hereafter (except specified). After obtaining the eigenenergies and the eigenstates, a number of quantities (the root-mean-square

radius, the one-body densities for the particle distribution, and the shape-densities) are further calculated. Thereby, inherent physics can be extracted, and a clear comparison among different kinds of system can be made. The emphasis is placed to demonstrate the universality of the PZ and the similarity among different systems. A short discussion on 4-fermion systems is also given at the end.

2 Universal prohibited zones in the coordinate space

The equilateral tetrahedron (ET) and the square (SQ) are the two most important geometries. We shall study the symmetry constraint taking place at the ET, SQ, and their neighborhoods. The zone associated with the extension-contraction of an ET along one of its two-fold (three-fold) axis is defined as Z_{2-2} (Z_{1-3}). Z_{2-2} and Z_{1-3} are related to the H-type and K-type of oscillations, respectively, that exist in tetramers.[20] When the tetrahedrons of Z_{2-2} are further twisted about the two-fold axis, the extended zone is defined as $Z_{\rm twi}$.

When appropriate degrees of freedom are chosen, the general expression Eq. (1) could have very simple form. For Z_{2-2}, let the Jacobi coordinates be $\mathbf{r}_a = \mathbf{r}_2 - \mathbf{r}_1$, $\mathbf{r}_b = \mathbf{r}_4 - \mathbf{r}_3$, $\mathbf{r}_c = (\mathbf{r}_4 + \mathbf{r}_3 - \mathbf{r}_2 - \mathbf{r}_1)/2$, then $\mathbf{r}_a \perp \mathbf{r}_b \perp \mathbf{r}_c$ and $r_a = r_b$ are required. r_a and r_c are considered as variable. We introduce a body frame Σ' with its origin at the c.m., its $\mathbf{k}'$ lying along $\mathbf{r}_c$, $\mathbf{j}'$ lying along $\mathbf{r}_a$, and $\mathbf{i}'$ lying along $\mathbf{r}_b$. Z_{2-2} is shown in Fig. 1a. This zone is 2-dimensional in Σ'.

In general, an eigenstate can be expressed by using the arguments of a body frame as

$$\Psi^{\Pi}_{LM}(X) = \sum_{Q} D^{L}_{QM}(\Omega)\Psi^{\Pi}_{LQ}(X'), \tag{2}$$

where X denotes the set of coordinates relative to a fixed frame Σ, and X' denotes the set relative to Σ', Ω denotes the set of Euler angles responsible for the transformation from Σ' to Σ.[21] Let P denotes an arbitrary particle permutation, I a space inversion with respect to the c.m., and $R^{\mathbf{v}}_{\phi}$ a rotation about the axis $\mathbf{v}$ by the angle ϕ. In Z_{2-2} we have the equivalence $IP \doteq R^{\mathbf{k}'}_{\pi/2}$. When IP act at the left side of Eq. (2) and $R^{\mathbf{k}'}_{\pi/2}$ acts at the right side, we obtain the constraint

$$(-i)^{Q}\Psi^{\Pi}_{LQ}(X') = \Pi\Psi^{\Pi}_{LQ}(X'), \tag{3}$$

which is a simple form of Eq. (1). Therefore, $\Psi^{\Pi}_{LQ}(X')$ is nonzero in Z_{2-2} only if $Q = 0, \pm 4, \cdots$ (when $\Pi = 1$), or $Q = \pm 2, \pm 6, \cdots$ (when $\Pi = -1$).

We have also the equivalence $IP \doteq R^{\mathbf{j}'}_{\pi}$, which leads to the second constraint

$$(-1)^{L+Q}\Psi^{\Pi}_{L,-Q}(X') = \Pi\Psi^{\Pi}_{LQ}(X'). \tag{4}$$

Therefore, the $Q = 0$ component exists only if $(-1)^L = \Pi$.

With this in mind, we know that Z_{2-2} is a PZ for 0^- and 1^- states (because they have only $|Q| \leq 1$ components), and for 1^+ and 3^+ states (because they do not have $|Q| \geq 4$ components and their $Q = 0$ component violates the requirement $(-1)^L = \Pi$).

When $r_c = r_a/\sqrt{2}$, the particles form an ET. The zone of ET is denoted as $Z_{\rm ET}$ which is one-dimensional in Σ' and is a subspace of Z_{2-2}. In $Z_{\rm ET}$ OA (refer to Fig. 1a) becomes a three-fold axis of an ET. Thus, additionally, we have

$$R^{\mathbf{OA}}_{2\pi/3} = R^{\mathbf{j}'}_{-\beta}R^{\mathbf{k}'}_{2\pi/3}R^{\mathbf{j}'}_{\beta} \doteq P, \tag{5}$$

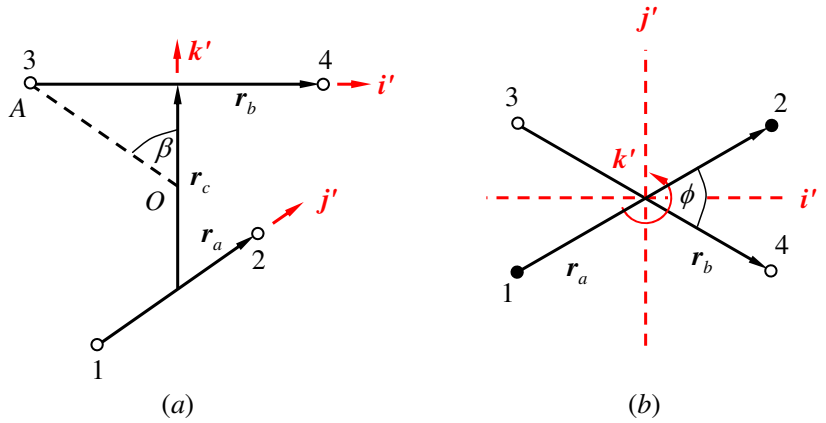

Fig. 1 (a) The zone Z_{2-2} defined in a body-frame with $\mathbf{r}_c$ lying along the third body-axis $\mathbf{k}'$, $\mathbf{r}_a$ lying along $\mathbf{j}'$, and $\mathbf{r}_b$ lying along $\mathbf{i}'$. $r_a = r_b$ is assumed. In this zone the magnitudes r_a and r_c are considered as variable. (b) The zone $Z_{\rm twi}$ defined in a body frame with $\mathbf{r}_c$ also lying along $\mathbf{k}'$, $\mathbf{r}_a \perp \mathbf{r}_c$ lying under the i'-j' plane, and $\mathbf{r}_b \perp \mathbf{r}_c$ lying above the i'-j' plane. $r_a = r_b$ and $\phi_a = -\phi_b$ are assumed. In this zone $r_c, r_a = r_b$, and $\phi = \phi_a - \phi_b$ are considered as variable.

where $\beta = \cos^{-1}(\sqrt{1/3})$ is the angle between OA and $\mathbf{k}'$. This leads to a set of homogeneous linear equations as

$$\sum_{Q'}[(\sum_{Q''} d^L_{Q'Q''}(-\beta)e^{-i\frac{2\pi}{3}Q''}d^L_{Q''Q}(\beta)) - \delta_{Q'Q}]\Psi_{LQ'}(\mathrm{ET}) = 0, \tag{6}$$

where $d^L_{Q'Q''}$ is the matrix elements of the rotation about $\mathbf{j}'$.[21] Under the constraints given by Eqs. (3), (4) and (6), nonzero solutions exist at the ET only if $L^{\Pi} = 0^+$, 3^- and 4^+ (if $L \leq 4$). They are called ET-accessible (ET-**ac**) states.[18,19]

When $r_c \to 0$, the shapes in Z_{2-2} tends to a SQ with its plane lying on the $\mathbf{i}'$-$\mathbf{j}'$ plane (Fig. 1a). The zone of SQ is denoted as $D_{\rm SQ}$ which is also one-dimensional in Σ'. For $D_{\rm SQ}$ we have $I \doteq P$. Thus, the SQ can only exist in $\Pi = +1$ states. As a subspace of Z_{2-2}, the SQ must be constrained by Eqs. (3) and (4). Thus the SQ-**ac** states are 0^+, 2^+ and 4^+ (if $L \leq 4$). Among them, 0^+ and 4^+ are both ET- and SQ-**ac**.

The geometries in Z_{1-3} are the regular trihedral pyramids. Let h denotes the height which is lying along the 3-fold axis of the pyramid, and s denotes the side length of the base regular triangle. h and s are variable. Let $\mathbf{k}'$ be lying along the 3-fold axis, and $\mathbf{j}'$ along a height of the base triangle. Then we have $R^{\mathbf{k}'}_{2\pi/3} \doteq P$ and $R^{\mathbf{i}'}_{\pi} \doteq IP$. Accordingly, Z_{1-3} is a PZ for 0^-, 1^+ and 2^- states.

In $Z_{\rm twi}$ (refer to Fig. 1b where $\mathbf{r}_c$ is lying along $\mathbf{k}'$ and can not be seen) $\mathbf{r}_a \perp \mathbf{r}_c$, $\mathbf{r}_b \perp \mathbf{r}_c$, $r_a = r_b$ are required. r_a, r_c and the angle ϕ between $\mathbf{r}_a$ and $\mathbf{r}_b$ are considered as variable. In this zone $\mathbf{k}'$ is a 2-fold axis, and $\mathbf{i}'$ lying along the bisector of ϕ is also a 2-fold axis. We have $R^{\mathbf{k}'}_{\pi} \doteq P$ and $R^{\mathbf{i}'}_{\pi} \doteq P$. Accordingly, $Z_{\rm twi}$ is a PZ for 1^- and 1^+ states.

For coplanar shapes, let $\mathbf{k}'$ be vertical to the plane of the shapes. Then, $R^{\mathbf{k}'}_{\pi} \doteq I$ must hold. We considered the following three cases.

(i) The coplanar shape is invariant under inversion (e.g., a parallelogram) and, accordingly, $\mathbf{k}'$ is a two-fold axis. The associated zone is denoted as D_A, and the equivalence $I \doteq P$ holds.

(ii) The shape contains at least a two-fold axis on the $\mathbf{i}'$-$\mathbf{j}'$ plane (say, an isosceles trapezoid). The zone is denoted as D_B, and the equivalence $R_\pi^{\mathbf{j}'} \doteq P$ holds.

(iii) The intersection of D_A and D_B, namely, $D_{A\cap B}$. This zone includes the rectangles and diamonds. Specifically, $D_{\rm SQ} \in D_{A\cap B}$.

Associated with the above zones, the PZ are summarized in Table 1. It is emphasized that the existence of the PZ is universal disregarding the kinds of 4-boson systems. Since the prohibition is absolutely not violable, the effect of the PZ is decisive. The features of all the eigenstates can be thereby more or less predicted. For examples, 0^+ is free from symmetry constraint. Thus, it can choose the structure most favorable to binding, and its wave function is expected to surround an ET. 2^+ is not ET-**ac** but is SQ-**ac**, therefore its wave function is expected to surround a SQ, and so on.

For the eight zones listed in Table 1, the most important zones are the $Z_{\rm ET}$ and $D_{\rm SQ}$. The accessibility of these two zones is crucial to the energies of the eigenstates as shown below. When a zone is accessible to a state but some subspaces inside the zone are not (say, $Z_{\rm twi}$ is accessible to 0^- but its subspace Z_{2-2} is not), the zone is not a stable zone because the PZ inside the zone implies the existence of inherent nodal surfaces, and therefore specific oscillations are excited (examples are given below).

Table 1 The prohibited zones (PZ) emerge in the coordinate space for the L^Π states ($L \leq 4$) of 4-boson systems. The second column gives the dimension of the zones in the body frame. The appearance of a PZ is marked by an "✓" (say, $Z_{\rm twi}$ is a PZ for 1^+ and 1^- states).

	dim	0^+	1^+	2^+	3^+	4^+	0^-	1^-	2^-	3^-	4^-
$Z_{\rm twi}$	3		✓					✓			
Z_{2-2}	2		✓		✓		✓	✓			
$Z_{\rm ET}$	1		✓	✓	✓		✓	✓	✓		✓
$D_{\rm SQ}$	1		✓		✓		✓	✓	✓	✓	✓
Z_{1-3}	2		✓				✓		✓		
D_A	3						✓	✓	✓	✓	✓
D_B	3		✓				✓				
$D_{A\cap B}$	2		✓				✓	✓	✓	✓	✓

3 Trapped 4-boson systems with three kinds of interaction

We are going to present numerical results to evaluate quantitatively the consequence of the PZ. It is assumed that the four particles are confined by an isotropic harmonic trap $\frac{1}{2}m\omega^2 r_i^2$. The trap is introduced just for supporting more bound states for a systematic analysis, and will not at all affect the appearance of the PZ found above. $\hbar\omega$ and $\sqrt{\hbar/m\omega}$ are used as units of energy and length. With these units three types of interactions are assumed: $V_{\rm A}(r) = 10(2e^{-(r/1.428)^2} - e^{-(r/2.105)^2})$, $V_{\rm B}(r) = 1000e^{-3r} - 40/r^6$ (when $r \geq 1.2$) and $V_{\rm B}(r) = V_{\rm B}(1.2)$ (when $r < 1.2$) , and $V_{\rm C}(r) = 15$ (when $r \leq 1$) and $V_{\rm C}(r) = 0$ (when $r > 1$), respectively, where $r = |\mathbf{r}_i - \mathbf{r}_j|$. $V_{\rm A}$ has a short-ranged character and was previously used in nuclear physics for the α-particles, $V_{\rm B}$ belongs to the Van der Waals type for atoms, while $V_{\rm C}$ is just a repulsive hard core potential. In fact, the three interactions are chosen quite arbitrary, just to show the possible similarity among different systems.

With the interaction and the trap, the Hamiltonian is

$$H = \sum_i (-\frac{1}{2}\nabla_i^2 + \frac{1}{2}r_i^2) + \sum_{i<j} V_J(|\mathbf{r}_i - \mathbf{r}_j|), \tag{7}$$

where $J = A, B$, or C. A set of basis functions is introduced to diagonalize the Hamiltonian to obtain the spectra and the eigenstates. The details are given in the Appendix A. Note that $V_{\rm A}$ and $V_{\rm B}$ both contain a minimum. Thus the total interaction energy would be lower if the particle separations are appropriate. Therefore the particles will pursue a better geometry. The ET (all six bonds can be optimized) and the SQ (four bonds can be optimized) with an appropriate size will be the first and second choices. However, for $V_{\rm C}$, the minimum is not contained, therefore the pursuit to a better geometry is less anxious.

4 Spectra

The spectra with the three types of interaction are plotted in Fig. 2. Although the interactions are very different, the three spectra have common features. From Table 1 we know that the 0^+, 2^+, 4^+, and 3^- are ET-**ac** and/or SQ-**ac**. They form the first group. This group of states are explicitly lower than the others, and the 0^+ state is the lowest as expected. Usually, the states with a larger L is higher due to having a stronger rotation energy. However, for $V_{\rm A}$ and $V_{\rm B}$, 2^+ is higher than 3^- because the former is simply SQ-**ac** while the latter is ET-**ac**. Nonetheless, for V_C, the superiority of ET over SQ is weaker, thereby the normal sequence in this group is recovered. For all the three spectra, 0^- and 1^+ are the highest because many PZ are contained. These two form the third group. Although they contain zero or seldom rotation energy, they are still much higher than the 4^+. This fact demonstrates the serious effect of the symmetry constraint. The remaining four states (1^-, 2^-, 4^-, and 3^+) are in the middle, they form the second group. Totally speaking, the two spectra for $V_{\rm A}$ and $V_{\rm B}$ are very similar (except the energy scale). The similarity of the spectrum of V_C to the other two is weaker.

5 Root mean square radius

We calculate the root mean square radius $r_{\rm rms}(L^\Pi)$ to evaluate the size of each state (refer to Appendix B). The ratios $r_{\rm rms}(L^\Pi)/r_{\rm rms}(0^+)$ are shown in Fig. 3 where the three dotted lines guiding the eyes go up and down in a synchronous way. It demonstrates once again the similarity among different systems. For all the three types of interactions, the sizes of the ET-**ac** states 0^+, 3^-, and 4^+ are relatively smaller, while the sizes of 0^- and 1^+ are the largest (because their wave functions are expelled from many PZ as shown below). If dynamic effect played an essential role, the largest would have $L = 4$ because the particles are pushing out by a stronger centrifugal force. But in fact not.

6 Particle distribution

The particle distributions in the $\Psi^\Pi_{L,L}$ states are shown by the one-body densities $r^2\rho_1(r,\theta)$, where r and θ are the magnitude and the polar angle of a position vector $\mathbf{r}$

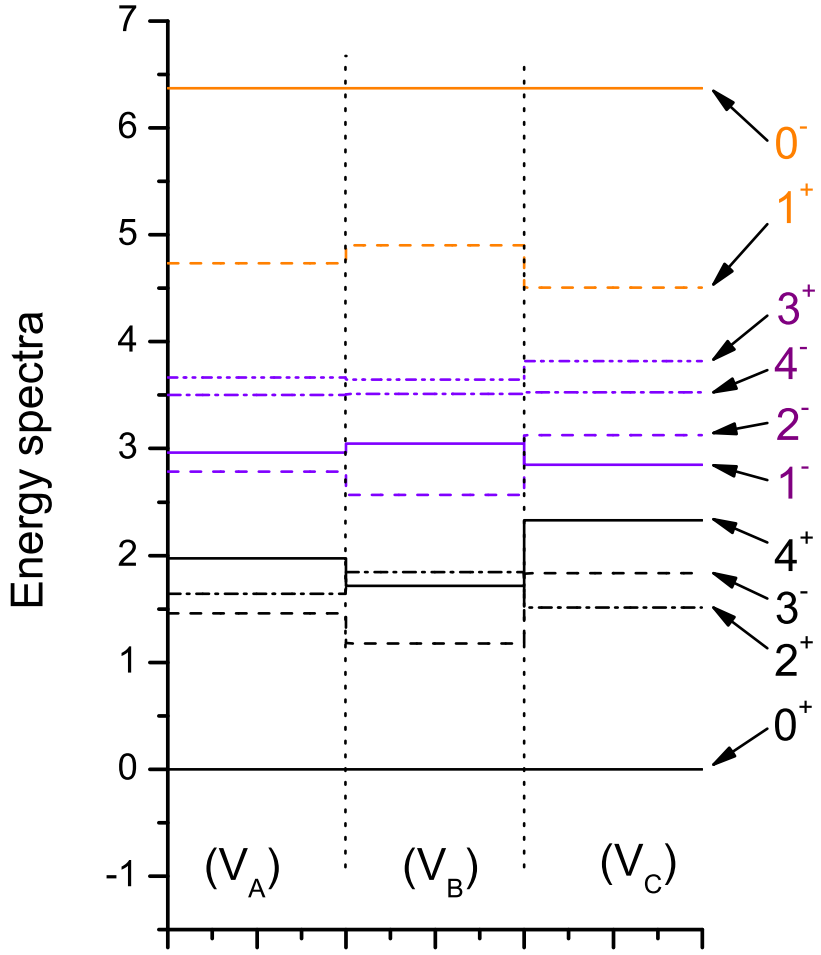

Fig. 2 Spectra of the 4-boson system with $L = 0$ to 4 and parity $\Pi = \pm 1$. Only the lowest one of a L^{Π}-series are given. Three types of interactions $V_{\rm A}$, $V_{\rm B}$, and $V_{\rm C}$ are considered. The levels have been shifted so that the three ground states (0^+) of the three types have energy zero. The energy unit for $V_{\rm A}$ is $\hbar\omega$. The energy units for the spectra of $V_{\rm B}$ and $V_{\rm C}$ have been redefined so that the three 0^- states have the same value of energy (but in different units). In all the three spectra, the lowest four belong to the first group, the highest two belong to the third group. The four in the middle belong to the second group. The states contained in the groups are the same for the three types without exception. In a group the same state is given by the same kind of line for the three types (say, all the 3^- states belonging to the first group are given by the dash-line).

originating from the c.m. (refer to Appendix B). They are shown in Figs. 4 and 5. In general the distribution depends on M. The choice $M = L$ implies that the Z-axis is chosen to be lying along the direction of L. In Fig. 4, 0^+ is isotropic as expected. 1^+ is nearly isotropic. 3^+ and 4^+ have a denser distribution when the particle is closer to the equator ($\theta \to \pi/2$). In general, when L is larger, the system will more prefer to increase its moment of inertia so as to reduce the rotation energy. This explains why 3^+ and 4^+ prefer to be a little flattened. On the contrary, the distribution of 2^+

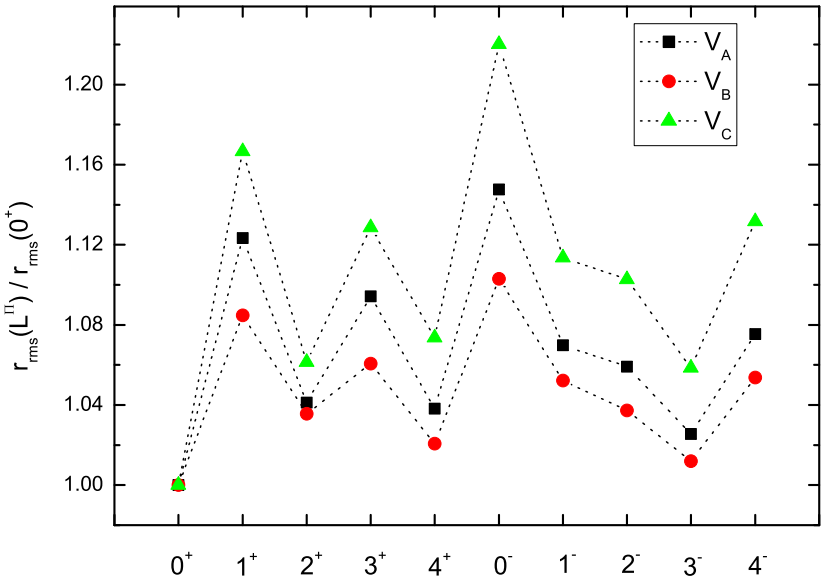

Fig. 3 The ratio $r_{\rm rms}(L^{\Pi})/r_{\rm rms}(0^+)$ for the L^{Π} states of the three types. Square is for the type $V_{\rm A}$, circle for $V_{\rm B}$, and triangle for $V_{\rm C}$.

prefers to be closer to the Z-axis. This is not due to dynamics but due to symmetry constraint. Since 2^+ is SQ-**ac** as shown in Table 1, it will pursue the SQ (This will be further confirmed later). When the Σ' as shown in Fig. 1 is adopted, $\mathbf{k}'$ is chosen to be vertical to the SQ . However, the SQ can only appear in $Q = 0$ component due to the constraint Eq. (3). In this component L is also nearly vertical to $\mathbf{k}'$, and therefore L and the SQ are nearly coplanar. Thus, in the choice $M = L$, SQ and the Z-axis are nearly coplanar. This explains why the equator is less preferred by 2^+. Furthermore, 4b is strikingly similar to 4a, 4c is also similar to 4a but in a less extent. Thus, the angular distribution of particle is not seriously affected by the details of interaction. In the following, we shall see once and once that the similarity between the cases with V_A and V_B is high, but weaker with V_C. It has been mentioned that, for V_C, the pursuit to a better geometry is less anxious. This cause the difference in the extent of similarity.

High similarity between the cases V_A and V_B emerges also in Fig. 5 for the odd-parity states.

7 Shape-densities

The similarity can be more clearly revealed by observing the wave functions directly. For this purpose, we introduce the hyper-radius $R \equiv \sqrt{\mu_a r_a^2 + \mu_b r_b^2 + \mu_c r_c^2}$, where $\mu_a = \mu_b = 1/2$ and $\mu_c = 1$ are the reduced masses. Note that R would remain invariant under the transformation between two sets of Jacobi coordinates. Therefore R is suitable for measuring the size. From the normality and from Eq. (2), integrating

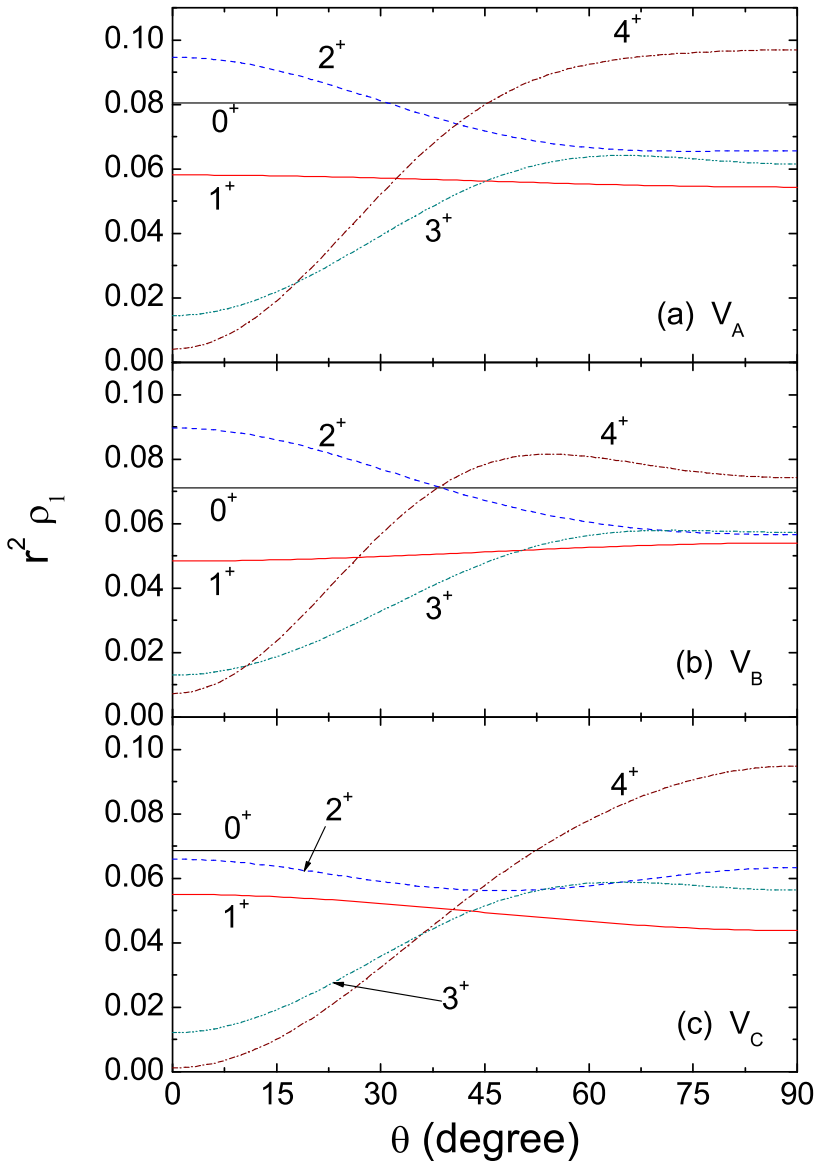

Fig. 4 One-body densities $r^2\rho_1(r,\theta)$ for the even parity states $\Psi^{(+)}_{LM}$ with r being fixed at $r_{\rm rms}(L^\Pi)$. $M=L$ is chosen. Since $\rho(r,\theta)=\rho(r,\pi-\theta)$, only $\theta\le\pi/2$ is included.

over the Euler angles, we have

$$1=\langle\Psi^\Pi_{LM}(X)|\Psi^\Pi_{LM}(X)\rangle=\frac{8\pi^2}{2L+1}\sum_Q\int {\rm d}X'|\Psi^\Pi_{LQ}(X')|^2. \tag{8}$$

There are six arguments included in X', one is R responsible for the size and the others are denoted by S responsible for the shape, and ${\rm d}X'=R^8{\rm d}R{\rm d}S$. Thus the normality

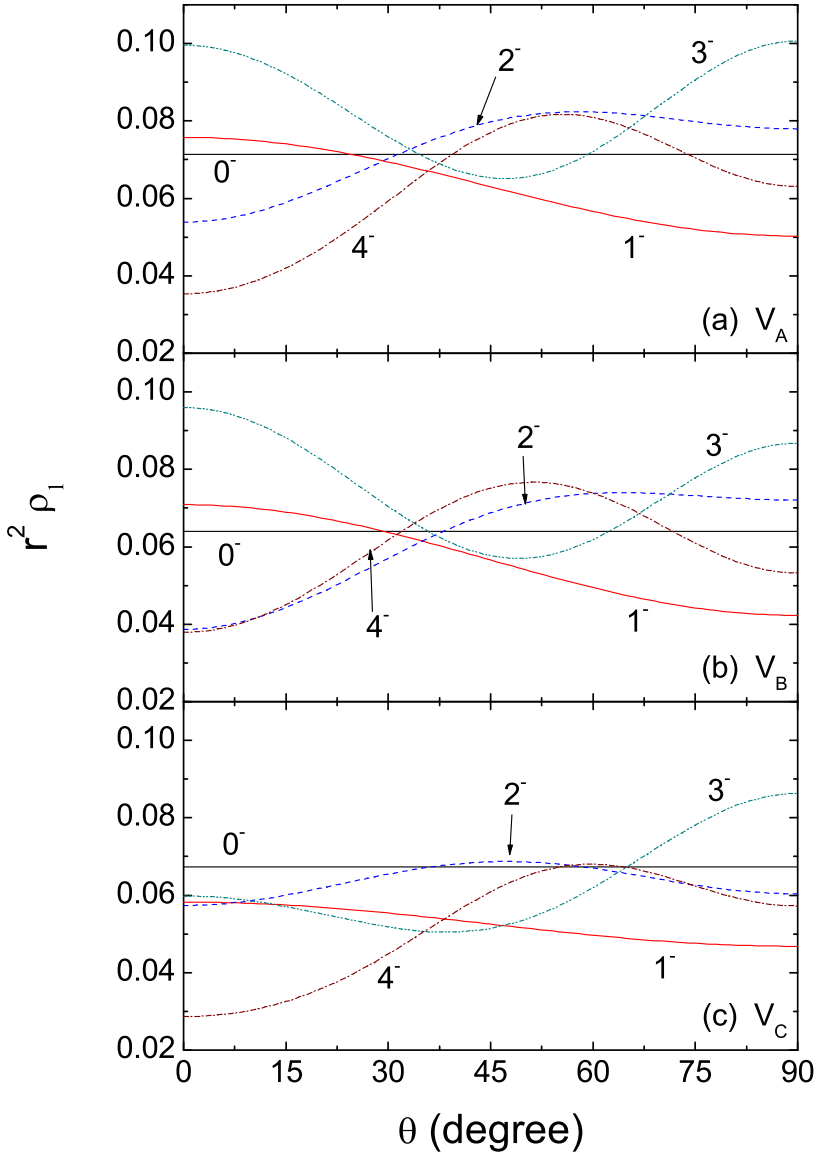

Fig. 5 Similar to Fig. 4 but for the odd parity states $\Psi^{(-)}_{LL}$.

can be rewritten as $1 = \int \mathrm{d}R\mathrm{d}S\ \rho(X')$, where

$$\rho(X') \equiv \frac{8\pi^2}{2L+1} R^8 \sum_Q |\Psi^{\Pi}_{LQ}(X')|^2, \tag{9}$$

is the probability density that the system has a given size and a given shape (while the orientation of the shape has already been integrated). Therefore $\rho(X')$ is called the shape-density.

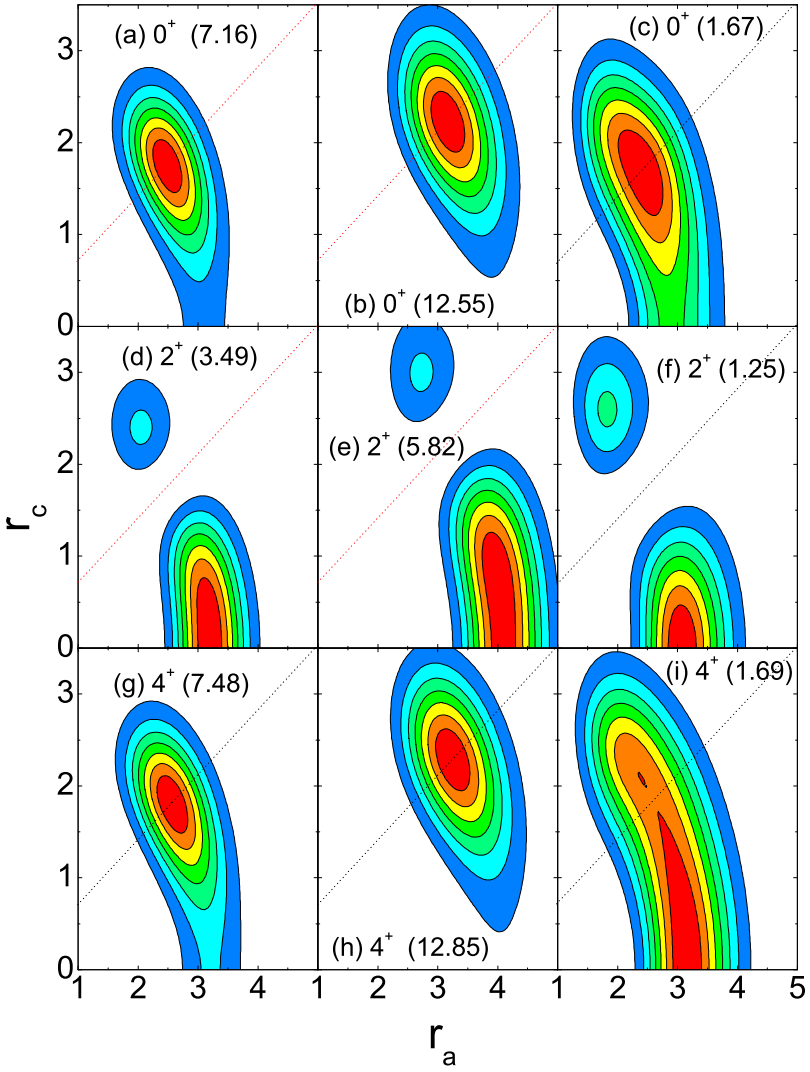

Fig. 6 The shape-densities $\rho(X')$ of even-parity states observed in Z_{2-2} (refer to Fig. 1a) as a function of r_a and r_c. The three rows are for $0^+, 2^+$, and 4^+. The three columns from left to right are for V_A, V_B, and V_C, respectively (the same for Figs. 6 to 9). The distribution of the density is relative to a body-frame, while the orientation of the body-frame has been integrated. The dotted lines have $r_c = r_a/\sqrt{2}$, they denote the ET shapes. In each panel, the value of the maximum is given inside a pair of parentheses, while the values of the contours form an arithmetic series and decrease to zero. In Fig.6 - 9 the unit of length is $\sqrt{\hbar/m\omega}$

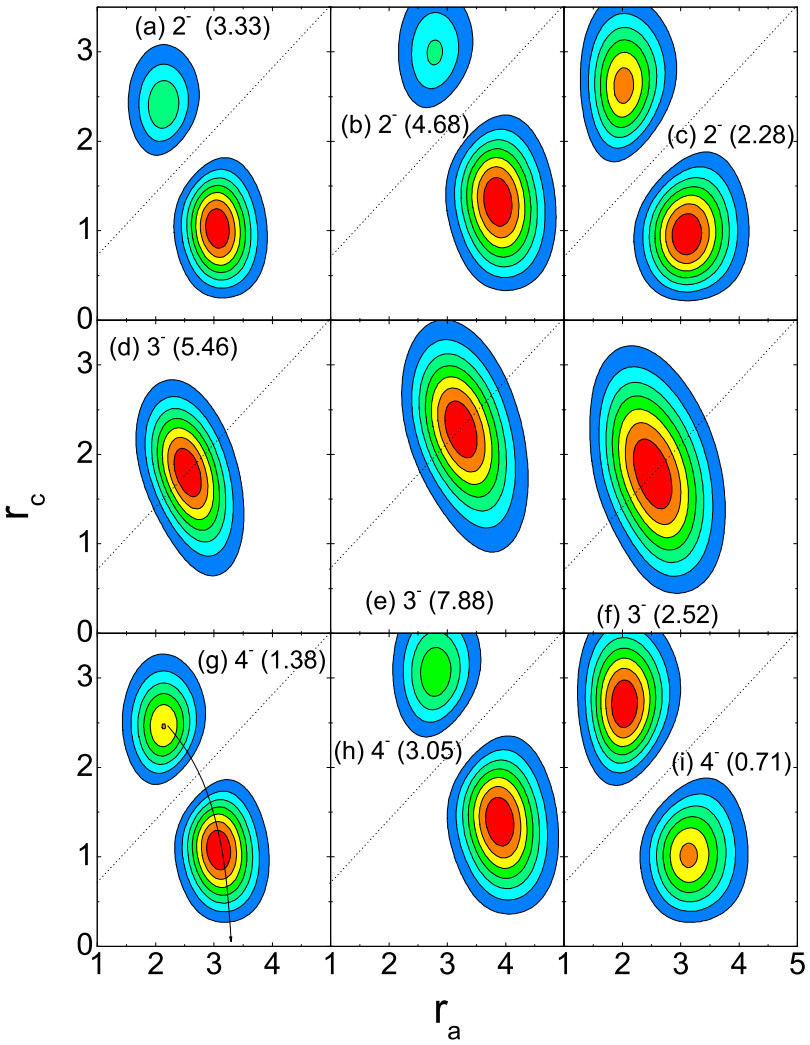

Fig. 7 The shape-densities $\rho(X')$ of odd-parity states 2^-, 3^-, and 4^-, respectively, observed in Z_{2-2} as a function of r_a and r_c. Refer to Fig. 6.

We shall observe $\rho(X')$ in some selected zones. Since the ET and the SQ are both contained in Z_{2-2}, this zone is important. $\rho(X')$ of the even-parity and odd-parity states observed in Z_{2-2} are given in Figs. 6 and 7, where r_a and r_c are variables. Since 1^+, 3^+, 0^-, and 1^- have their wave functions absolutely being zero in this zone, they do not appear in these figures (refer to Table 1, where Z_{2-2} is a PZ for them). Thus the states appear in the figures are 0^+, 2^+, 4^+, 2^-, 3^-, and 4^-. Note that the 0^+ state is both ET-**ac** and SQ-**ac**. Due to the superiority of the ET over the SQ, all the peaks in 6a, 6b, and 6c (for V_A, V_B, and V_C) are peaked at an ET (where $r_c = r_a/\sqrt{2}$) but not a SQ (where $r_c = 0$). It has been mentioned that, for V_C, the pursuit to a better geometry

is less anxious. Accordingly, the distribution in 6c extends considerably toward a SQ . 4^+ is also both ET-**ac** and SQ-**ac**. The SQ of the 4^+ can be nearly vertical to its L because $|Q| = 4$ component is allowed (refer to Eq. (3)). Thereby the moment of inertia can be increased and the rotation energy can be reduced. Accordingly, for 4^+, the SQ becomes more competitive. In fact, for V_C, the SQ has replaced the ET as the most probable shape as shown in 6i.

3^- is ET-**ac** but not SQ-**ac**. Accordingly, the distribution is more concentrated around the ET and away from the SQ as shown in Figs. 7d, 7e, and 7f.

2^+ is not ET-**ac** but SQ-**ac**. Accordingly, the distribution is more concentrated around the SQ as shown in Figs. 6d, 6e, and 6f.

Among the four states of the second group, 2^- and 4^- are allowed to appear in this zone, and are shown in the first and third rows of Fig. 7. They are neither ET-**ac** nor SQ-**ac**. There are two peaks in each panel, the peak with a smaller r_c is the higher peak (except in Fig. 7i). It implies that the most probable shape is a compressed ET along one of its two-fold axis.

In general, one can define a specific degree of freedom (accordingly, a specific 1-dimensional curve in the coordinate space) to describe a specific mode of oscillation. When a wave function is remarkably distributed along the curve then the specific mode is involved. If a node appears at the curve, the oscillation has been excited. If more nodes appear along the curve, the excitation is more vigorous (the simplest example is referred to the one-dimensional harmonic oscillator states). In each panel, let a curve starting from the upper peak (a prolonged ET), extending to the lower peak, and then extending to the abscissa (refer to the solid curve added in Fig. 7g). Accordingly, r_c decreases along $\mathbf{k}$ (refer to Fig. 1a) and the prolonged ET suffers a compression and is transformed to a SQ. Once r_c becomes zero, this process will continue but in reverse direction (namely, r_c increases further along $-\mathbf{k}$). Then, the SQ is transformed back to a prolonged ET, and repeatedly. The mode associated with the transformation is named the ET-SQ-ET mode (or the H-type oscillation named in [20]). Since the wave functions of 2^- and 4^- appear as nodes at the ET and SQ, the ET-SQ-ET mode contains three nodes and therefore is an excited mode. This explains why 2^- and 4^- are considerably higher than 2^+ and 4^+.

From Table 1 we know that Z_{1-3} is a PZ for 2^- but not for 4^-. Thus the increase of rotation energy in 4^- can be partially compensated due to the Z_{1-3}-**ac**. Therefore, the energy difference between 2^- and 4^- is small. In fact, the wave function of 4^- is also remarkably distributed in Z_{1-3}. Say, for V_C, the maximum of $\rho(X')$ of 4^- in Z_{1-3} is equal to 1.52 located at a flattened regular pyramid, whereas the maximum in Z_{2-2} is equal to 0.71 located at a prolonged ET (shown in Fig. 7i). Thus, for V_C, the most probable shape of 4^- is the flattened pyramid instead of the prolonged ET.

The other two member 1^- and 3^+ of the second group do not appear in Z_{2-2}. From the spectra for V_A and V_B, we know that 1^- is higher than 2^-, and 3^+ is higher than 4^-. This fact implies that the prohibition of Z_{2-2} will lead to an increase in energy. From Table 1 we know that both 1^- and 3^+ will be distributed in Z_{1-3}. This is shown in Fig. 8a-8c and 8d-8f, respectively. In all the panels, there are two peaks. The upper peak has larger s (i.e., the base triangle is larger), and is associated with a flattened regular pyramid, while the lower peak a prolonged pyramid. Let a curve be defined connecting the two peaks. This curve is associated with the transformation between the flattened and prolonged pyramid (or the K-type of oscillation [20]). Since a node appears at the curve (more exactly, at an ET), this oscillation has been excited. Also from Table 1 we know that coplanar structures might exist in these two states.

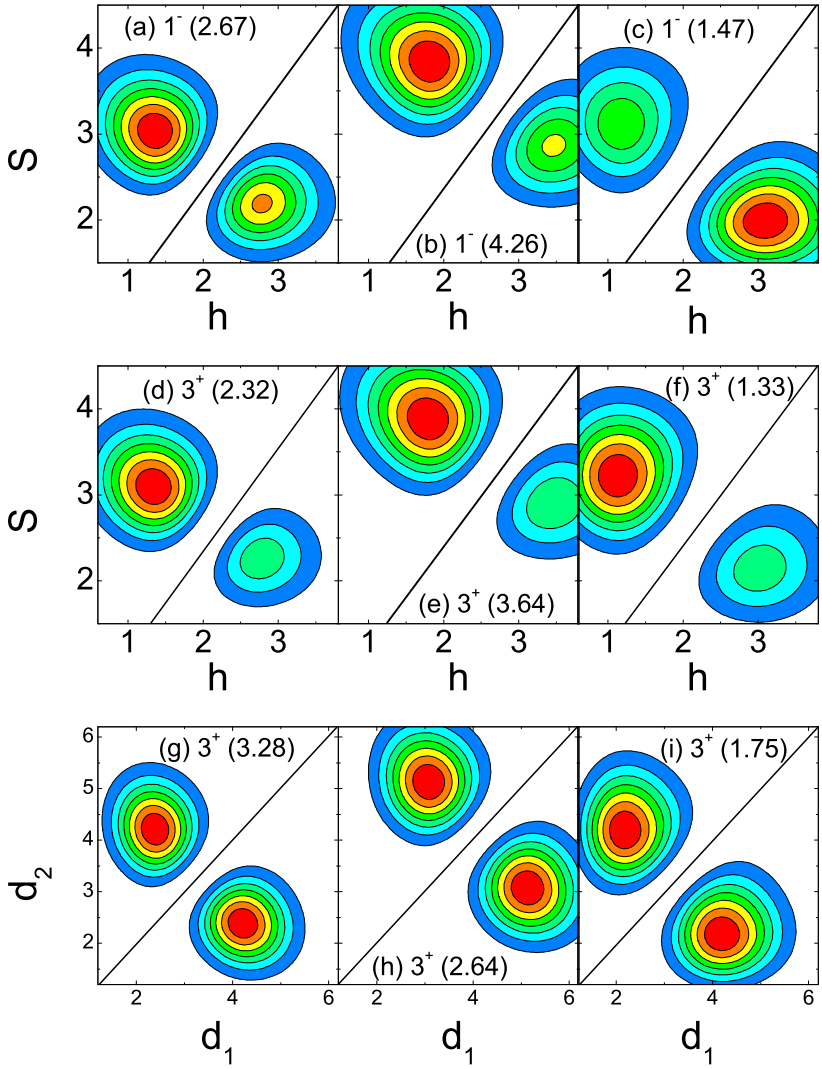

Fig. 8 $\rho(X')$ of 1^- (a-c) and 3^+ (d-f) plotted in Z_{1-3} for the regular pyramids. The height h of the pyramid and the side-length s of the base triangle are variables. The straight lines having $h = \sqrt{2/3}s$ are associated with an ET, and they are an inherent nodal line for these states. $\rho(X')$ of 3^+ plotted in $D_{A\cap B}$ (g-i), where d_1 and d_2 are the two diagonals of a rhombus. The straight line $d_1 = d_2$ is associated with the SQ, and it is an inherent nodal line for 3^+.

This is shown in Figs.8g-8i, where the two peaks are associated with a flattened and a prolonged diamond, and a node appears between them. Thus an excited oscillation of a diamond around a SQ is contained.

For the 0^- state of the third group any coplanar structures are prohibited. This is due to the equivalence $R_\pi^{\mathbf{k}'} \doteq I$, where $\mathbf{k}'$ is chosen to be vertical to the plane ($R_\pi^{\mathbf{k}'}$ causes no effect on $L = 0$ states, while I causes a change of sign on odd parity states,

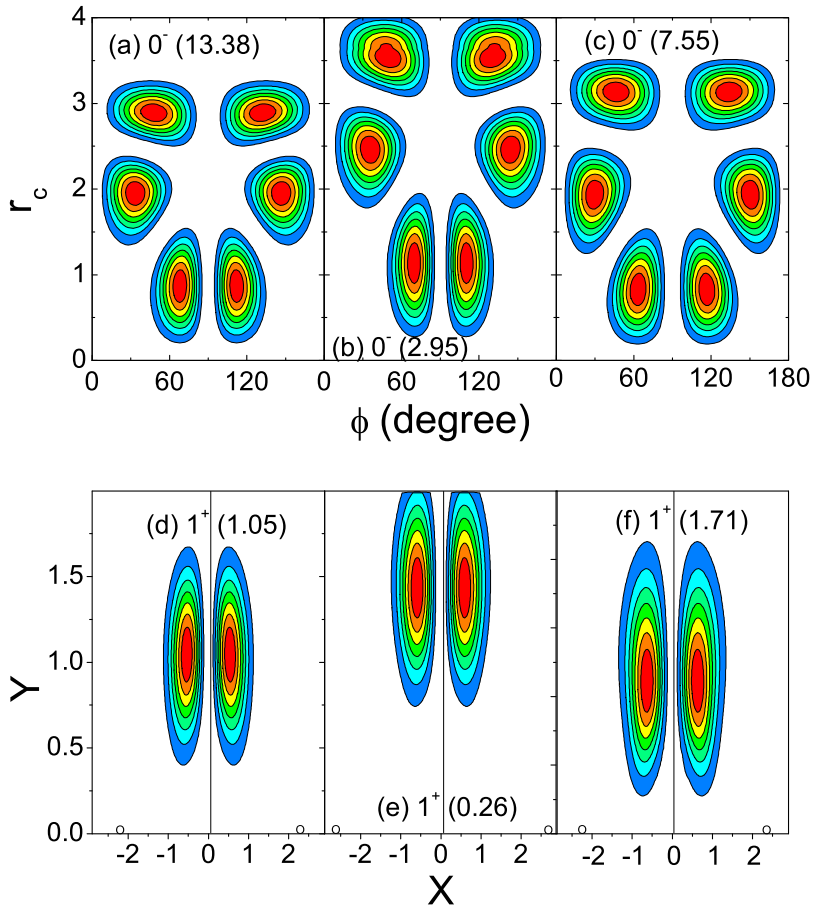

Fig. 9 (a-c) $\rho(X')$ of 0^- plotted in a subspace of $Z_{\rm twi}$ (refer to Fig. 1b), where r_c and ϕ are variables, and $r_a = r_b$ depends on r_c via a constraint that the hyper-radius $R \equiv \sqrt{\mu_a r_a^2 + \mu_b r_b^2 + \mu_c r_c^2}$ is fixed at $2r_{\rm rms}$ (p.s., for an ET, this constraint implies that the distance of each particle from the c.m. is $r_{\rm rms}$). (b) $\rho(X')$ of 1^+ plotted in D_A for the parallelograms. This zone is a plane. The X- and Y-axes of a body frame with its origin located at the c.m. is plotted. Two particles are given lying at the X-axis marked by two small circles. The other two have coordinates (x, y) and $(-x, -y)$. The peaks represent the most probable locations of the third particle (while the fourth particle at the lower plane can not be seen). Accordingly, the most probable shape is a parallelogram. The vertical line at $x = 0$ represents the diamonds, and is an inherent nodal line for 1^+.

this leads to a contradiction) Thus, from Table 1, the wave function of 0^- would be essentially distributed in $Z_{\rm twi}$. However, many subspaces in $Z_{\rm twi}$ are PZ of 0^-. This is shown in Figs. 9a-9c. Where $\phi = 0$ and π, and $r_c = 0$ are three nodal lines because they are associated with coplanar shapes (refer to Fig. 1b). $\phi = \pi/2$ is also a nodal line because the associated shape belongs also to Z_{2-2} which is prohibited. Furthermore, let the coordinates of the particle 2 relative to Σ' be denoted as (x, y, z). Accordingly, those of the particles 1, 3, and 4 are $(-x, -y, z)$, $(-x, y, -z)$, and $(x, -y, -z)$, respectively.

One can see that, if $y = z$ the equivalence $R_{\pi}^{\mathbf{j}'} I R_{\pi/2}^{\mathbf{i}'} \doteq P$ holds (where P is an interchange of a pair of particles), if $z = x$ the equivalence $R_{\pi}^{\mathbf{k}'} I R_{\pi/2}^{\mathbf{j}'} \doteq P$ holds, and if x=y the equivalence $R_{\pi}^{\mathbf{i}'} I R_{\pi/2}^{\mathbf{k}'} \doteq P$ holds. For 0^-, the left side of each of the equivalence will cause a change of sign while the right side does not. Therefore 0^- must be zero in each of the subspace with $y = z$, $z = x$, or $x = y$. The equality $y = z$ can be rewritten as $r_c/r_a = \sin(\phi/2)$. Note that r_c and r_a are constrained as $\sqrt{r_a^2 + r_c^2} = 2r_{\rm rms}$ in Figs. 9a-9c. Thus $r_c = 2r_{\rm rms}\sin(\phi/2)/\sqrt{1+\sin^2(\phi/2)}$ is a nodal line. Similarly, the case z=x leads to the nodal line $r_c = 2r_{\rm rms}\cos(\phi/2)/\sqrt{1+\cos^2(\phi/2)}$, while the case x=y leads to the nodal line $\phi = \pi/2$ mentioned above. Totally, six nodal lines are contained in Figs. 9a-9c. These lines expel the wave function from favorable zones and cause strong inherent oscillation. This explains why the energy of 0^- is so high.

For 1^+, due to the prohibition of $Z_{\rm twi}$ and Z_{1-3}, the structure of tetrahedron is unfavorable. Furthermore, due to the prohibition of D_B, the coplanar structures are also unfavorable. It was found that this state is a mixture of a parallelogram and a deformed tetrahedron. The shape-density surrounding the parallelogram is shown in Fig.s 9d-9f, where the vertical line is associated with the diamonds and is a nodal line for 1^+. The two peaks (each peaked at a parallelogram) separated by the nodal line implies an excited oscillation of the parallelogram.

From the shape-densities plotted in Figs. 6 to 9, the decisive effect of the PZ is clearly shown. Since the PZ is universal, the wave functions are expelled in a universal way, and the room left for dynamic adjustment is limited. This leads to similarity which is clearly shown by comparing the three patterns of any row in the figures for V_A, V_B, and V_C, respectively.

8 Fermion systems

The existence of PZ is not only for 4-boson systems but for all kinds of few-body systems containing identical particles. For an example of a 4-fermion system, it is assumed that the spin-dependent interaction tends to align the spins (alternatively, a magnetic field is applied so that the spins are aligned). For this case, the spatial wave functions will be fully anti-symmetric. Accordingly, the equivalent operation Eq. (3) that hold in Z_{2-2} leads to the fact that $\Psi_{LQ}(X')$ is nonzero only if $Q = 0, \pm 4, \cdots$ (when $\Pi = -1$), or $Q = \pm 2, \pm 6, \cdots$ (when $\Pi = 1$). In particular, the $Q = 0$ component exists only if $\Pi = -1$ and L being even. Accordingly, the ET-**ac** states are now 0^-, 3^+, and 4^-. The SQ-**ac** states are now 2^+, 3^+, and 4^+, while the states rejected from Z_{2-2} are now 0^+, 1^+, 1^-, and 3^-. Among them 1^+ and 3^- can both access Z_{1-3}, while 1^+ can access also coplanar structures. Therefore, for the ten states under consideration, we can predict that 0^-, 2^+, 3^+, and 4^- would be the lowest, while 1^- and 0^+ would be the highest. We repeat our previous calculation for the case V_A but using fully anti-symmetric basis functions. The resultant spectra is shown in Table 2.

The result in Table 2 confirms the prediction.

9 Final remarks

From the point of classical dynamics, it is incredible that there are zones in the coordinate space favorable in energy but absolutely prohibited. However, this paper demon-

Table 2 The energies of the ten states (in ascending order) of the fermion system calculated with $V_{\rm A}$ (the unit is $\hbar\omega$).

State	0^-	3^+	2^+	4^-	1^+	2^-	3^-	4^+	1^-	0^+
Energy	0	0.97	1.37	1.77	1.95	2.15	2.89	2.93	3.22	4.03

strates analytically and numerically that this is a fact in microscopic few-body systems. Since the prohibition arises from the symmetry constraint which depends only on the inherent symmetry but is irrelevant to dynamics, the existence of the PZ is universal disregarding the kinds of systems and the details of interaction. The quantum states of different systems will have exactly the same PZ located at the same subspace when these states are governed by the same inherent symmetry (namely, they belong to the same set of representations of the symmetry groups). Since some of the PZ have a higher geometric symmetry, they are the zones more favorable in energy. Therefore, the prohibition causes serious effect and destroys thoroughly the picture painted simply by dynamics. Consequently, the structures of the low-lying states are decisively determined by their inherent symmetry, and the room left for the adjustment from dynamics is narrow, in particular for the $i = 1$ states

Although only 4-body systems with [1,1,1,1] and $[1^4]$ symmetries are concerned in this paper, obviously the existence of the PZ is a universal phenomenon for all kinds of few-body systems with identical particles.

Acknowledgment: The support from the NSFC under the grant No.10874249 is appreciated.

Appendix

A Diagonalization of the Hamiltonian

When the c.m. coordinates have been removed, the Hamiltonian for internal motion $H_{\rm int}$ can be expressed by a set of Jacobi coordinates $\mathbf{r}_a = \mathbf{r}_2 - \mathbf{r}_1$, $\mathbf{r}_b = \mathbf{r}_4 - \mathbf{r}_3$, and $\mathbf{r}_c = (\mathbf{r}_3 + \mathbf{r}_4 - \mathbf{r}_1 - \mathbf{r}_2)/2$. Let

$$h(\mu, \mathbf{r}) \equiv -\frac{1}{2\mu}\nabla^2_{\mathbf{r}} + \frac{1}{2}\mu r^2, \tag{10}$$

which is the Hamiltonian of harmonic oscillation, Then

$$H_{\rm int} = h(1/2, \mathbf{r}_a) + h(1/2, \mathbf{r}_b) + h(1, \mathbf{r}_c) + \sum_{i<j} V(|\mathbf{r}_j - \mathbf{r}_i|). \tag{11}$$

Let us introduce a variational parameter γ. The eigenstates of $h(\gamma, \mathbf{r})$ are denoted as $\phi^{\gamma}_{nl}(\mathbf{r})$, where n and l are the radial and angular quantum numbers, respectively. From $\phi^{\gamma}_{nl}(\mathbf{r})$ a set of basis functions for the 4-body system is defined as

$$\Phi^{\gamma}_{k,\Pi LM}(1234) \equiv [(\phi^{\gamma/2}_{n_a l_a}(\mathbf{r}_a)\phi^{\gamma/2}_{n_b l_b}(\mathbf{r}_b))_{l_{ab}}\phi^{\gamma}_{n_c l_c}(\mathbf{r}_c)]_{LM}, \tag{12}$$

where l_a and l_b are coupled to l_{ab}, then l_{ab} and l_c are coupled to the total orbital angular momentum L and its Z-component M, Π the parity, k denotes the set of quantum numbers.

These functions should be further symmetrized. For bosons, l_a and l_b should be even and we define

$$\tilde{\Phi}^{\gamma}_{k,\Pi LM} \equiv \sum_{p} \Phi^{\gamma}_{k,\Pi LM}(p_1 p_2 p_3 p_4), \tag{13}$$

where the right side is a summation over the permutations. Making use of the Talmi-Moshinsky coefficients, [22,23,24] each term at the right can be expanded in terms of $\Phi^{\gamma}_{k}(1234)$. For an example,

$$\Phi^{\gamma}_{k,\Pi LM}(1324) = \sum_{k'} A^{\Pi L}_{kk'} \Phi^{\gamma}_{k',\Pi LM}(1234), \tag{14}$$

where $A^{\Pi L}_{kk'}$ is the Talmi-Moshinsky coefficients which can be obtained by using the method given in the ref.[24]. Note that the set $\{\tilde{\Phi}^{\gamma}_{k,\Pi LM}\}$ has not yet been orthonormalized. Thus a standard procedure is needed to perform to transform $\{\tilde{\Phi}^{\gamma}_{k,\Pi LM}\}$ to a orthonormalized set $\{\tilde{\tilde{\Phi}}^{\gamma}_{q,\Pi LM}\}$, where q is a serial number to denote a basis function, and each basis function can be expanded in terms of $\{\Phi^{\gamma}_{k,\Pi LM}(1234)\}$. Finally, the set $\{\tilde{\tilde{\Phi}}^{\gamma}_{q,\Pi LM}\}$ is used to diagonalize $H_{\rm int}$. Due to the Talmi-Moshinsky coefficients, only the set of coordinates $\mathbf{r}_a$, $\mathbf{r}_b$, and $\mathbf{r}_c$ is involved. Thus the calculation of the matrix elements is straight forward. When Π and L are given, a series of states will be obtained after the diagonalization. The lowest one of the series is called the first state. γ has to be adjusted so that the energy of the first state is as low as possible.

Due to having a trap, the bound states will tend to zero quite fast when r tends to infinity. For this case, the above basis functions are suitable and will lead to a better convergency. Let $N_{abc} = 2(n_a + n_b + n_c) + l_a + l_b + l_c$, and let the number of basis functions be constrained by $N_{abc} \leq N_{max}$. Then, as an example of the bosonic case, the resultant energy of the lowest 0^+ state with the interaction V_A is 2.2965, 2.2961, and 2.2960 $\hbar\omega$, respectively, when $N_{max} = 16$, 18, and 20. Since the emphasis is placed at the qualitative aspect, the convergency appears to be satisfactory.

B One-body density $r^2\rho_1$, the root mean square radius $r_{\rm rms}$

After the diagonalization, each eigenstate $\Psi^{\Pi,i}_{L,M}$ is expanded in terms of $\tilde{\tilde{\Phi}}^{\gamma}_{q,\Pi LM}$, where i denotes the i-th state of the (ΠL)-series. For convenience, a transformation from the set $\tilde{\tilde{\Phi}}^{\gamma}_{q,\Pi LM}\}$ to the set $\{\Phi^{\gamma}_{k,\Pi LM}(1234)\}$ is made, and the eigenstate is re-expanded as $\Psi^{\Pi,i}_{L,M} = \sum_k C^{\gamma i \Pi L}_{k} \Phi^{\gamma}_{k,\Pi LM}(1234)$. In order to extract the information of a particle from $\Psi^{\Pi,i}_{L,M}$, another set of Jacobi coordinates $\mathbf{r}_a = \mathbf{r}_2 - \mathbf{r}_1$, $\mathbf{r}_d = (\mathbf{r}_1 + \mathbf{r}_2)/2 - \mathbf{r}_4$, and $\mathbf{r}_e = \mathbf{r}_3 - (\mathbf{r}_4 + \mathbf{r}_1 + \mathbf{r}_2)/3$ is defined. Accordingly, we have the basis function

$$\Upsilon^{\gamma}_{k,\Pi LM}(1234) \equiv [(\phi^{\gamma/2}_{n_a l_a}(\mathbf{r}_a)\phi^{2\gamma/3}_{n_b l_b}(\mathbf{r}_d))_{l_{ab}} \phi^{3\gamma/4}_{n_c l_c}(\mathbf{r}_e)]_{LM}. \tag{15}$$

Since the set $\{\Phi^{\gamma}_{k,\Pi LM}(1234)\}$ and the set $\{\Upsilon^{\gamma}_{k,\Pi LM}(1234)\}$ can be transformed into each other via the Talmi-Moshinsky coefficients, the eigenstate can once again expanded as

$$\Psi^{\Pi,i}_{L,M} = \sum_{k} D^{\gamma i \Pi L}_{k} \Upsilon^{\gamma}_{k,\Pi LM}(1234), \tag{16}$$

where the coefficients $D^{\gamma i \Pi L}_{k}$ can be known from the diagonalization and from the transformation between sets of basis functions.

Now, from the normality, we have

$$\begin{aligned} 1 &= \int \mathrm{d}\mathbf{r}_e \mathrm{d}\mathbf{r}_a \mathrm{d}\mathbf{r}_d (\Psi^{\Pi,i}_{L,M})^* \Psi^{\Pi,i}_{L,M} \\ &= \int \mathrm{d}r \ \sin\theta \mathrm{d}\theta \\ &\quad [2\pi(\frac{4}{3})^3 r^2 \int \mathrm{d}\mathbf{r}_a \mathrm{d}\mathbf{r}_d \sum_{k',k} D^{\gamma i \Pi L}_{k'} D^{\gamma i \Pi L}_{k} (\Upsilon^{\gamma}_{k',\Pi LM}(1234))^* \Upsilon^{\gamma}_{k,\Pi LM}(1234)], \end{aligned} \tag{17}$$

where θ is the polar angle of $\mathbf{r}_e$, and $r = \frac{3}{4}r_e$ is the distance of particle 3 from the c.m. Obviously, the quantity inside the bracket is just the one-body density $r^2\rho_1(r,\theta)$ describing the particle distribution (all the four particles are distributed in the same way).

The root mean square radius is

$$r_{\rm rms} = \frac{3}{4}(\sum_{k',k} D^{\gamma i\Pi L}_{k'} D^{\gamma i\Pi L}_{k} \langle \Upsilon^{\gamma}_{k',\Pi LM}(1234)|r_e^2|\Upsilon^{\gamma}_{k,\Pi LM}(1234)\rangle)^{1/2}. \quad (18)$$

References

1. Skorniakov, G. V., Ter-martirosian, K. A. Three-body problem for short-range forces 1, Scattering of low-energy neutron by deuterons. *Sov. Phys. JETP*, **4**, 648 (1957).
2. Danilov, G. S. On the three-body problem with short-range forces. *Sov. Phys. JETP*, **13**, 349 (1961).
3. Phillips, A. C. Consistency of the low-energy 3-nucleon observables and the separable interaction model. *Nucl. Phys. A* **107**, 209 (1968).
4. Efimov, V. Energy levels arising from resonant two-body forces in a three-body system. *Phys. Lett.* **B33**, 563 (1970).
5. Efimov, V. Weakly-bound states of three resonantly-interacting particles. *Sov. J. Nucl. Phys.* **12**, 589 (1971).
6. Rutherford, D. E. *Substitutional Analysis* (Edinburgh University Press, Edinburgh, 1948).
7. Racah, G. *Group Theory and Spectroscopy* (Princeton University Press, Princeton, NJ, 1951).
8. Lobel, E. M. *Group Theory and its Applications*, Vols.1,2, and 3 (Academic Press, New York, 1968, 1971, and 1975).
9. Elliott, J. P. & Dawber, P. G. *Symmetry in Physics*, Vols.1,2 (McMillan Press, London, 1979).
10. Bao, C. G. Comparison of the structures of an atomic three-valence-electron system with a nuclear three-valence-neutron system. *Few-Body Systems* **13**, 41 (1992).
11. Bao, C. G. Possible modes of internal motions in a 3-electron model system - the $^2S^e$ states. *Z. phys. D: At., Mol. Clusters* **22**, 557 (1992).
12. Bao, C. G. Possible modes of angular motion in ^4S degrees triply excited states. *J. Phys. B: At. Mol. Opt. Phys.* **25**, 3725 (1992).
13. Bao, C. G. Modes of angular motion in intrashell $^{2S+1}S^o$ states of four-valence-electron atomic systems. *Phys. Rev. A* **47**, 1752 (1993).
14. Bao, C. G. & Yang, X. Z. & Lin, C. D. Nodal structures of intrashell states of three-valence-electron atoms. *Phys. Rev. A* **55**, 4168 (1997).
15. Bao, C. G. Qualitative feature of the low-lying intrashell states of 4-valence-electron atoms derived from symmetry consideration. *Phys. Lett. A* **250**, 123 (1998).
16. Morishita, T. & Lin, C. D. Classification and rovibrational normal modes of 3l3l ' 3l " triply excited states of atoms. *Phys. Rev. A* **64**, 052502 (2001).
17. Poulsen, M. D. & Madsen, L. B. Classification of atomic states by geometrical and quantum-mechanical symmetries. *Phys. Rev. A* **72**, 042501 (2005).
18. Bao, C. G. Inherent nodal structures of the wavefunctions of a 4-boson system. *Chin. Phys. Lett.* **14**, 20 (1997).
19. Bao, C. G. & Li, X. G. & Xie, W. F. Analysis of the Structure of Low-Lying States of Four-Boson Systems Based on Symmetry. *Few-Body Systems* **23**, 201 (1998).
20. Hadizadeh, M. R., Yamashita, M. T., Tomio, L., Delfino, A., Frederico, T. Binding and structure of tetramers in the scaling limit. *Phys. Rev. A*, **85**, 023610 (2012).
21. Edmonds, A. R. *Angular Momentum in Quantum Mechanics* (Princeton University Press, Princeton, NJ, 1957).
22. Brody, T. A. & Moshinsk, M. *Table of transformation Brackets*, (Universidad Nacional Autonoma de Mexico, Monografias del Instituto de Fisica, 1960).
23. Baranger, M. & Davies, K. T. R. Oscillator brackets for Hartree-Fock calculations. *Nucl. Phys.* **79**, 403 (1966).
24. Tobocman, W. A generalized Talmi-Moshinsky transformation for few-body and direct interaction matrix elements. *Nucl. Phys. A* **357**, 293 (1981).